Symmetry breaking in self-assembled monolayers on solid surfaces: Anisotropic surface stress

W. Lu* and Z. Suo
Mechanical and Aerospace Engineering Department and Princeton Materials Institute, Princeton University, Princeton, New Jersey 08544

(Received 15 June 2001; published 15 January 2002)

This paper models the self-assembly dynamics of a two-phase monolayer on an elastic substrate. The two phases coarsen to reduce the phase boundary energy and refine to reduce the elastic energy. To minimize the total free energy, the two phases can order into nanoscale patterns. We combine the continuum phase field model of spinodal decomposition and the anisotropic surface stress. The numerical simulation shows various patterns, such as interwoven stripes, parallel stripes, triangular lattice of dots, and herringbone structures. The surface stress anisotropy causes a transition from the parallel stripes to the herringbone structures. We show that this symmetry breaking mesophase transition obeys the classical theory of Landau.

DOI: 10.1103/PhysRevB.65.085401 PACS number(s): 68.43.Hn

I. INTRODUCTION

For two decades, the invention of the scanning tunneling microscopy (STM) and other probes has stimulated the studies of nanoscale activities on solid surfaces. An intriguing finding is the self-assembly of monolayer atoms on solid surfaces into nanoscale structures.[1–4] Atoms deposited on a low-symmetry surface of the substrate can self-assemble into quite different patterns. For instance, a submonolayer of oxygen on a Cu (110) surface can form stable periodic stripes of alternating oxygen overlayer and bare copper, about 10 nm in width and running in the $\langle 001 \rangle$ direction.[5] This paper and the sequels present a model that predicts pattern types according to various kinds of anisotropy.

The atoms in the epilayer are usually stressed, even when the epilayer and substrate are of the same kind of atoms. The surface stress, with a unit of force per length, can be roughly viewed as the residual stress times the layer thickness.[6–8] The surface stress can be obtained from experimental measurements[7,8] or from first-principles calculations.[9,10] The surface stress is a second-rank tensor. The anisotropy of the surface stress need not be coupled with that of the substrate elasticity. Depending on the epilayer and substrate, surface stress anisotropy can still be significant when the substrate has a highly symmetric crystal structure and is almost elastically isotropic. Surface stress anisotropy plays an important role in surface reconstruction[11,12] and accounts for the domain patterns on reconstructed silicon (100) surface.[13,14] The model of Alerhand *et al.*[13] highlights two competing effects: surface stress anisotropy and domain wall energy. Narasimhan and Vanderbilt[15] applied the same concept to model the herringbone reconstruction of the Au (111) surface.[16]

A binary epilayer differs from a single-crystal surface in several aspects. In the former case, surface stress nonuniformity originates from compositional modulation, rather than structural variation. More importantly, the entropy of mixing and the enthalpy of mixing play roles, along with the surface stresses and phase boundaries. The entropy of mixing may be potent enough to stabilize a uniform epilayer.

We have recently proposed a continuous phase model.[17,18] Unlike Vanderbilt and co-workers,[13,15] we do not preassume the pattern types. Our model is a dynamic model, and the material system can generate whatever patterns it favors. A sharply defined phase boundary adopted by Vanderbilt and co-workers is unsuitable for such a purpose. A phase boundary in our model is represented by a concentration gradient, an approach analogous to the work of Cahn and Hilliard on spinodal decomposition.[19] The continuous phase field model allows us to study the dynamic process of growing a superlattice from a disordered initial concentration distribution. The dynamics is particularly important in a system of many equilibrium configurations due to translational and rotational symmetries, leading to mesoscale defects in the superlattice. The advantage of phase field model and its application in other systems have been discussed before, e.g., Refs. 20 and 21.

We have performed linear perturbation analysis, studied the early stage of self-assembly behavior, and given the condition for the existence of a uniform epilayer.[18] We have also simulated the entire self-assembly process and discussed the effect of average concentration, guided self-assembly by initial conditions, and numerical technique in a series of papers.[22–24] Our previous papers have focused on the isotropic surface stress. In this paper we demonstrate how the anisotropy of the surface stress breaks the symmetry of the system and generates a variety of new patterns. In particular, we show a second-order mesophase transition from parallel stripes to herringbone structures. We assume here that the elastic substrate is isotropic; the effects of anisotropic elastic constants and anisotropic domain walls will be studied in the sequels to this paper.

II. CONTINUOUS PHASE FIELD MODEL WITH ANISOTROPIC SURFACE STRESS

Consider an epilayer composed of two kinds of atoms *A* and *B* on a substrate of atoms *S*. Here *A* and *B* can be both different from *S*, such as sulfur-silver mixture on a ruthenium substrate.[1] Alternatively, only one species of the epilayer is different from that of the substrate, such as oxygen atoms on a copper substrate.[5] As shown in Fig. 1, the epilayer is taken to be an infinitely large surface and the substrate a semi-infinite elastic body. The substrate occupies the half space $x_3 < 0$ and is bounded by the x_1-x_2 plane.

 ©2002 The American Physical Society

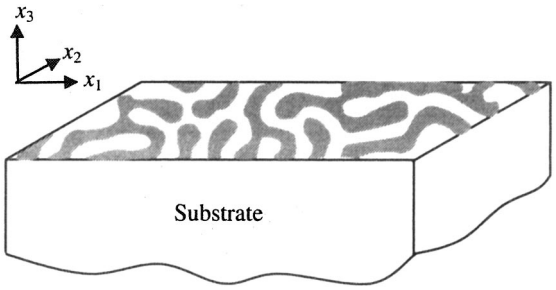

FIG. 1. Self-organized nanoscale patterns of an epilayer on a solid surface. The substrate occupies the half space $x_3<0$ and is bounded by the x_1-x_2 plane.

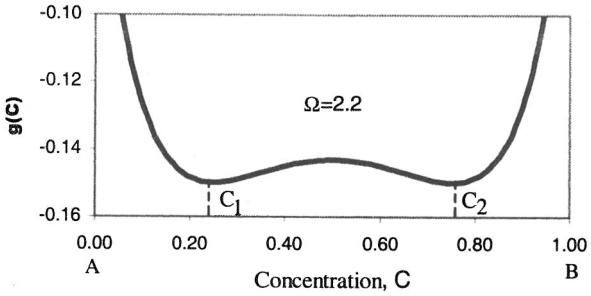

FIG. 2. The curve of $g(C)$ for $\Omega=2.2$. The double wells correspond to the two phases.

The free energy of the system comprises the surface energy in the epilayer and the elastic energy in the substrate. Focusing on the anisotropy of surface stress, we assume in this paper that the substrate is elastic isotropic. As usual, the elastic energy per unit volume in the bulk is a quadratic function of strain with Young's modulus E and Poisson's ratio ν as parameters.[23] The surface energy per unit area, Γ, takes an unusual form in our model. Define concentration C by the fraction of atomic sites on the surface occupied by species B. We will simulate the annealing process, in which the deposition process has stopped, but atoms are allowed to diffuse within the epilayer. Regard the concentration as a spatially continuous and time-dependent function $C(x_1,x_2,t)$. Assume that Γ is a function of the concentration C, the concentration gradient $C_{,\alpha}$ and the strain in the surface $\varepsilon_{\alpha\beta}$. A Greek subscript runs from 1 to 2. The strain tensor relates to the displacement gradient in the usual way as in the theory of elasticity. Expanding the function $\Gamma(C,C_{,\alpha},\varepsilon_{\alpha\beta})$ in the leading-order terms of the concentration gradient $C_{,\alpha}$ and the strain $\varepsilon_{\alpha\beta}$, we have

$$\Gamma = g + hC_{,\alpha}C_{,\alpha} + f_{\alpha\beta}\varepsilon_{\alpha\beta}, \tag{1}$$

where g, h, and $f_{\alpha\beta}$ are all functions of the concentration C. We have assumed that h is isotropic in the plane of the surface. The leading-order term in the concentration gradient is quadratic because, by symmetry, the term linear in the concentration gradient does not affect the surface energy. We have neglected terms quadratic in the strain, which relate to the excess in the elastic stiffness of the epilayer relative to the substrate.

When the concentration field is uniform in the epilayer, the substrate is unstrained and $g(C)$ is the only remaining term in Eq. (1). Hence $g(C)$ represents the surface energy per unit area of a uniform epilayer on an unstrained substrate. To describe phase separation, we prescribe $g(C)$ as any function with double wells. In numerical simulations, to be definite, we assume that the epilayer is a regular solution so that the function takes the form

$$g(C) = \Lambda kT[C\ln C + (1-C)\ln(1-C) + \Omega C(1-C)]. \tag{2}$$

The usual expression of $g(C)$ also includes a term linear in the concentration C, representing the weighted contribution of free energy by pure component A and B on the substrate. However, due to mass conservation, the average concentration is constant when atoms diffuse within the epilayer. Hence the term linear in C does not influence diffusion and is neglected here. The first two terms in the brackets result from the entropy of mixing and the third term from the enthalpy of mixing. Λ is the number of atoms per unit area on the surface, k is Boltzmann's constant, and T is the absolute temperature. The dimensionless number Ω measures bond strength relative to the thermal energy kT. When $\Omega<2$, the function $g(C)$ is convex. When $\Omega>2$, the function $g(C)$ has double wells. Figure 2 shows the $g(C)$ graph for $\Omega=2.2$. The double-welled $g(C)$ function drives phase separation; it favors neither coarsening nor refining.

We assume that $h(C)$ is a positive constant, $h(C)=h_0$. Any nonuniformity in the concentration field by itself increases Γ. In the phase field model, the second term in Eq. (1) represents the phase boundary energy. The total phase boundary energy of all the phase boundaries reduces when the two phases enlarge and the net length of the phase boundary reduces. Consequently, the concentration gradient term in Eq. (1) drives phase coarsening.

The quantity $f_{\alpha\beta}$, known as the surface stress tensor, is the surface energy change associated with the elastic strain.[25] As stated in the previous section, the concentration-dependent surface stress drives phase refining. We may assume that the surface stress is a linear function of the concentration, i.e., $f_{\alpha\beta}(C)=\psi_{\alpha\beta}+\phi_{\alpha\beta}C$, where $\psi_{\alpha\beta}=\psi_{\beta\alpha}$ and $\phi_{\alpha\beta}=\phi_{\beta\alpha}$ are material constants; see review in Ref. 8.

Atoms diffuse within the epilayer to reduce the combined surface energy and the elastic energy in the substrate. The corresponding diffusion equation is[22,23]

$$\frac{\partial C}{\partial t} = \frac{M}{\Lambda^2}\nabla^2\left(\frac{\partial g}{\partial C} - 2h_0\nabla^2 C + \phi_{\alpha\beta}\varepsilon_{\alpha\beta}\right), \tag{3}$$

where M is the mobility of atoms in the epilayer. The first two terms in Eq. (3), which are analogous to those in Cahn,[26] come from the free energy of mixing and the phase boundary energy. The third term comes from the concentration-dependent surface stress and from substrate elasticity. A repeated index implies summation.

When the concentration is nonuniform, the surface stress $f_{\alpha\beta}$ is also nonuniform. A stress field σ_{ij} is generated in the substrate, subject to the boundary conditions $\sigma_{3\alpha}=f_{\alpha\beta,\beta}$ and $\sigma_{33}=0$ at the boundary of $x_3=0$.[17] A Latin subscript runs from 1 to 3. The elastic field in a half space due to a tangen-

tial point force acting on the surface was solved by Cerruti.[27] The strain field in the surface, $\varepsilon_{\alpha\beta}$, can be obtained by linear superposition, resulting singular integrals over the entire surface:

$$\varepsilon_{\alpha\beta}=\frac{1+\nu}{\pi E}\int\int\frac{1}{\rho_3}\Bigg[\left(\nu-\frac{1}{2}\right)(\phi_{\beta\kappa}(x_\alpha-\xi_\alpha)+\phi_{\alpha\kappa}(x_\beta-\xi_\beta)) + \phi_{\gamma\kappa}\nu\left(\delta_{\alpha\beta}-\frac{3}{\rho^2}(x_\alpha-\xi_\alpha)(x_\beta-\xi_\beta)\right)(x_\gamma-\xi_\gamma)\Bigg] \times\frac{\partial C}{\partial\xi_\kappa}d\xi_1 d\xi_2, \tag{4}$$

where $\rho=\sqrt{(x_1-\xi_1)^2+(x_2-\xi_2)^2}$.

We define two length scales. A comparison of the first two terms in the parentheses of Eq. (3) defines a length:

$$b=\left(\frac{h_0}{\Lambda kT}\right)^{1/2}. \tag{5}$$

In the Cahn-Hilliard model this length scales the distance over which the concentration changes from the level of one phase to that of the other. That is, b is comparable to the thickness of the phase boundary. The magnitude of h_0 is on the order of energy per atom at a phase boundary. Using magnitudes $h_0\sim10^{-19}$ J, $\Lambda\sim5\times10^{19}$ m^{-2}, and $kT\sim5\times10^{-21}$ J (corresponding to $T=400$ K), we have $b\sim0.6$ nm.

The other length scale, which reflects the competition between coarsening and refining [the second and third terms in Eq. (3)], is defined by

$$l=\frac{Eh_0}{(1-\nu^2)\phi_{11}^2}. \tag{6}$$

Young's modulus of a bulk solid is about $E\sim10^{11}$ N/m^2. According to the data compiled in Ibach,[8] a representative value of slope of the surface stress is $\phi_{11}\sim4$ N/m. The equilibrium phase size is on the order $\sim4\pi l$, according to theoretical analysis and simulation.[18,23] These magnitudes, together with $h_0\sim10^{-19}$ J, give $4\pi l\sim8$ nm, which broadly agrees with observed phase sizes in experiments. A dimensionless parameter Q is defined by the ratio of the two length scales:

$$Q=\frac{b}{l}=\frac{(1-\nu^2)\phi_{11}^2}{E(\Lambda kTh_0)^{1/2}}. \tag{7}$$

The effect of the surface stress is negligible when $Q\to0$.

From Eq. (3), disregarding a dimensionless factor, we note that the diffusivity scales as $D\sim MkT/\Lambda$. To resolve events occurring over the length scale of b, the time scale is $\tau=b^2/D$, namely,

$$\tau=\frac{h_0}{M(kT)^2}. \tag{8}$$

Surface stress is a second-rank tensor, having two principal directions within the plane of the epilayer. The substrate being assumed elastically isotropic, we can always rotate the coordinates so that the shear component of the surface stress disappears. Hence we can set $\phi_{12}=0$ without losing generality. Define

$$r=\phi_{22}/\phi_{11}. \tag{9}$$

This parameter measures the degree of anisotropy.

The singular integrals in Eq. (4) make it inefficient to solve Eq. (3) in real space. An alternative, more efficient, method is to solve the equation in reciprocal space. The Fourier transform converts the integral-differential equation (3) into a regular partial differential equation. The integration operation, as well as the differentiation over space, is removed and the evolution equation can be dramatically simplified. It is not necessary to transform the expression of $\varepsilon_{\alpha\beta}$ in Eq. (4) into reciprocal space, which seems to be a formidable task. Alternatively, we transform the boundary conditions and solve the elasticity problem in reciprocal space directly. The result is very simple, as given below.

Let k_1 and k_2 be the coordinates in reciprocal space. Denote the Fourier transform of $C(x_1,x_2,t)$ by $\hat{C}(k_1,k_2,t)$, namely,

$$\hat{C}(k_1,k_2,t)=\int_{-\infty}^{\infty}\int_{-\infty}^{\infty}C(x_1,x_2,t)e^{-i(k_1x_1+k_2x_2)}dx_1dx_2. \tag{10}$$

Normalize Eq. (3) by b and τ, and apply the Fourier transform on both sides. We obtain the evolution equation in reciprocal space:

$$\frac{\partial\hat{C}}{\partial t}=-k^2\hat{P}-2(k^4-Qs)\hat{C}. \tag{11}$$

Here k and s are given by

$$k=\sqrt{k_1^2+k_2^2} \tag{12}$$

and

$$s=\frac{k_1^2(k^2-\nu k_1^2)+k_2^2(k^2-\nu k_2^2)r^2-2\nu k_1^2k_2^2r}{(1-\nu)k}. \tag{13}$$

When the surface stress is isotropic, $r=1$ and $s=k^3$, which reduce to the result in Ref. 23. $\hat{P}(k_1,k_2,t)$ is the corresponding form of $P(x_1,x_2,t)$ in reciprocal space, where

$$P(C)=\ln\left(\frac{C}{1-C}\right)+\Omega(1-2C). \tag{14}$$

The term $P(C)$ comes from the derivative of Eq. (2) with respect to C. The factor ΛkT disappears due to the normalization. Note that $P(C)$ is a function of x_1, x_2, and t. Because $P(C)$ is a nonlinear function of C, an analytical expression for $\hat{P}(k_1,k_2,t)$ is unavailable. The fast Fourier transform (FFT) and the inverse FFT are used in each time step. Details can be found in one of our previous papers.[23]

III. SIMULATIONS OF EVOLVING PATTERNS

A. Refining effect of the surface stress

Figure 3 shows two evolution sequences from $t=0$ to $t=1.0\times10^6$, the time unit being τ. The calculation cell size is $256b\times256b$. In the simulation, we take $\Omega=2.2$ and $\nu=0.3$. For sequence (a), there is an isotropic surface stress ($r=1$ and $Q=1$); for sequence (b), there is no surface stress ($Q=0$). The initial conditions are the same for the two sequences: the concentration has an average 0.5 and fluctuates randomly within 0.001 from the average. Boundary conditions of the calculation cell are periodic. Results are visualized by gray scale graphs in the (x_1,x_2) plane. The brighter region corresponds to the higher concentration, and the darker region corresponds to the lower concentration.

In sequence (a), shortly after phase separation, the two phases form interwoven stripes. The width of the stripes stabilizes very fast. From $t=1000$ to $t=1.0\times10^6$, the widths are almost invariant. The patterns resemble experimental observations.[4] By contrast, in sequence (b), the two phases try to increase their sizes as much as possible, restricted only by mass conservation and the size of the calculation cell. The system finally evolves into a state such that one phase takes half of the calculation cell and the other phase takes the other half. This reproduces the classical spinodal decomposition.[19] Comparison between the two cases clearly demonstrates the refining effect of surface stress.

Figure 4(a) is the pattern at $t=1.0\times10^6$, sequence (a) of Fig. 3. Figure 4(b) shows the concentration profile along the segment between the two arrows in Fig. 4(a). It is observed that the concentration is roughly 0.85 at the crest and 0.15 at the trough. Nonuniform concentration in the epilayer generates a strain field in the substrate. Figure 4(c) shows the strain field ε_{11} in the substrate. The brighter region corresponds to contraction, and the darker region corresponds to extension. (Here we take $\phi_{11}>0$.) Figure 4(d) gives a simple explanation. The traction on the surface is $\sigma_{31}=\partial f_{11}/\partial x_1=\phi_{11}\partial C/\partial x_1$, as shown in Fig. 4(d). The strain field in the substrate is caused by the traction. Figure 4(c) shows that the deformation is localized in a very shallow region close to the surface, decaying quickly along the $-x_3$ direction. The figure clearly shows the existence of a fringe elastic field in the substrate.

Sequence (a) in Fig. 3 can be roughly divided into three stages: phase separation, size selection, and spatial ordering. As shown in the sequence, the two phases reach equilibrium concentrations on the time scale of ~10. The time to attain a uniform size is on the order of 100–1000. The ordering of the structure still continues and is far from completion after $t=10^6$. It is relatively fast for the phases to separate, attain their equilibrium compositions, and select a uniform size, but very slow to order over a long distance. Our calculation shows that the system has the lowest energy if the stripes line up into parallel stripes.[23] However, due to the high symmetry of the system, all the directions are energy equivalent. The phases are confused and do not know which direction to line up. The interwoven stripes have been observed in many self-assembled systems, including block copolymers, ferromagnetic films, and the Langmuir monolayers.[28]

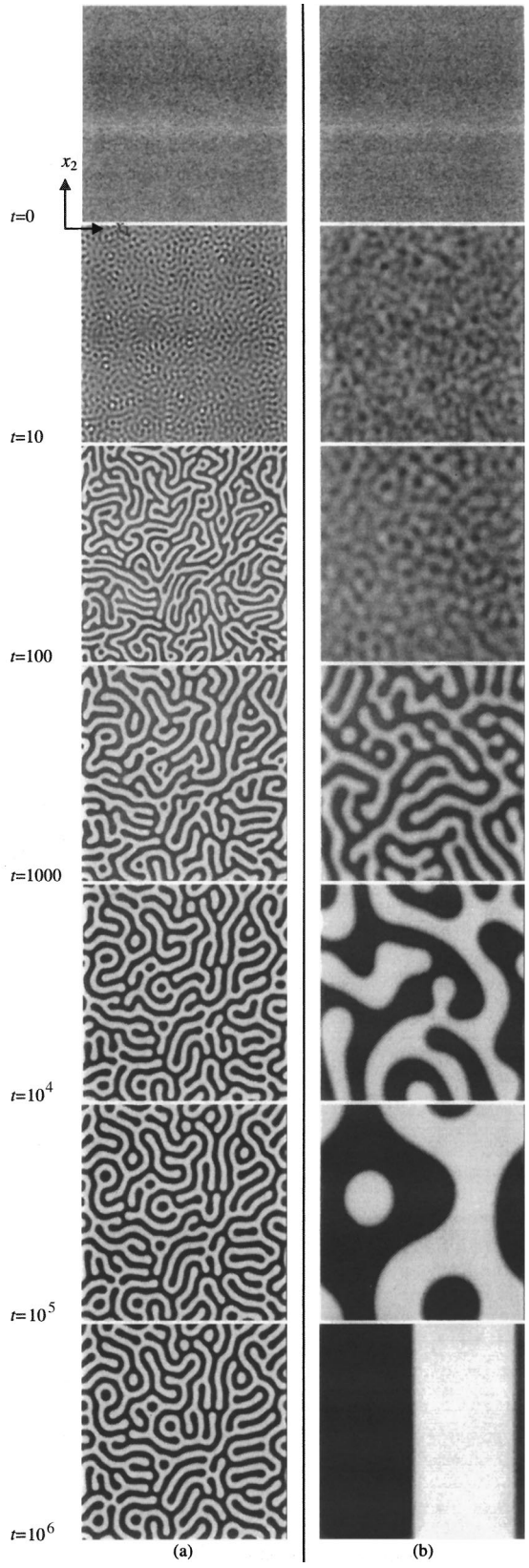

FIG. 3. Two evolution sequences. The time unit in the figures is τ. For sequence (a), there is isotropic surface stress; for sequence (b), there is no surface stress.

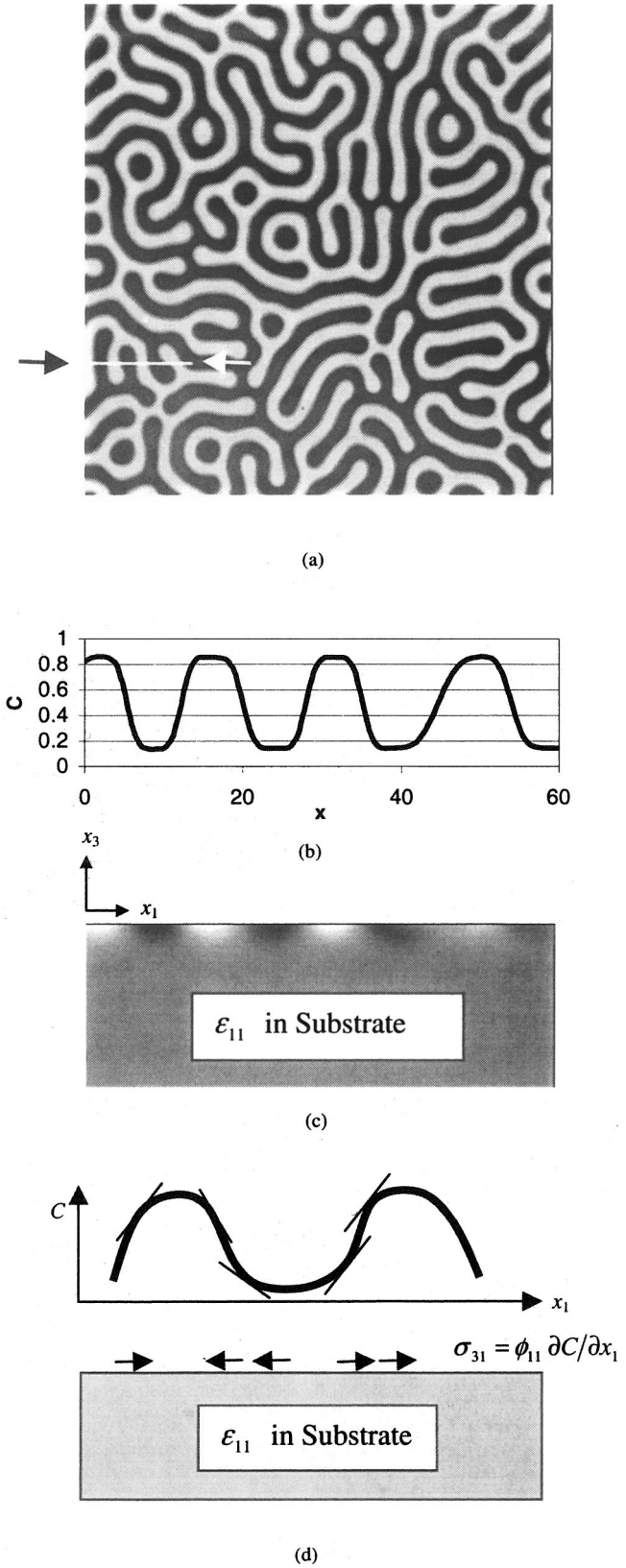

FIG. 4. (a) The pattern at $t=1.0\times10^6$. (b) The concentration profile along the segment between the two arrows in (a). (c) The corresponding strain field ε_{11} in the substrate. The brighter region corresponds to contraction, and the darker region corresponds to extension ($\phi_{11}>0$). (d) An explanation of the strain in the substrate.

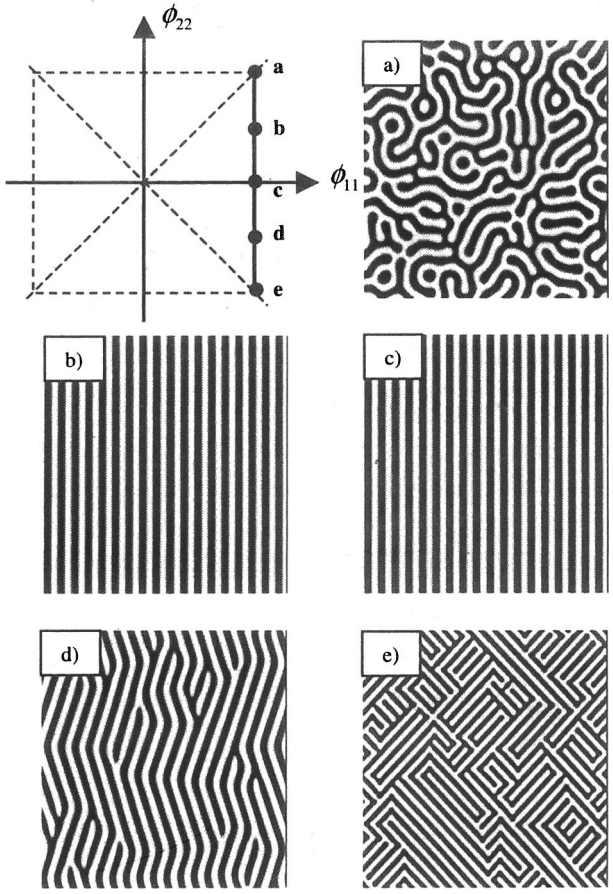

FIG. 5. Various patterns at $t=2.0\times10^5$ under five representative status of surface stress anisotropy. The average concentration is 0.5.

B. Symmetry breaking by the surface stress anisotropy

The slopes of the two principal surface stresses, ϕ_{22} and ϕ_{11}, play equivalent roles. Because the free energy of the system is quadratic in ϕ_{22} and ϕ_{11}, when they both change signs, the free energy is invariant. Consequently, we need only consider the region on the (ϕ_{11},ϕ_{22}) plane bounded by the two lines $\phi_{11}-\phi_{22}=0$ and $\phi_{11}+\phi_{22}=0$, as shown in Fig. 5. The five representative states **a**, **b**, **c**, **d**, and **e** correspond to $r=1$, 0.5, 0, -0.5, and -1, respectively. Figures 5(a)–5(e) show the simulated patterns at $t=2.0\times10^5$. All five simulations start from the same random initial condition as that in Fig. 3. State **a** corresponds to isotropic surface stress. Due to the high symmetry of the surface stress, the patterns exhibit a structure of high symmetry. Our simulation has shown that the interwoven structure still exists at $t\sim10^7$. This is probably the reason that interwoven stripes are commonly observed in many self-assembled systems.

The ordering process can be accelerated by suitably breaking the symmetry of the system. Our previous work has shown that by adding some lines to the random initial condition to provide a direction to line up the stripes, the formation of parallel stripes can be dramatically accelerated.[23] Figures 5(b) and 5(c) show how the anisotropy of surface stress has a similar effect. The anisotropy provides a direction preference, and the phases very quickly line up into periodic strips. The simulation shows that stripes form normal to the

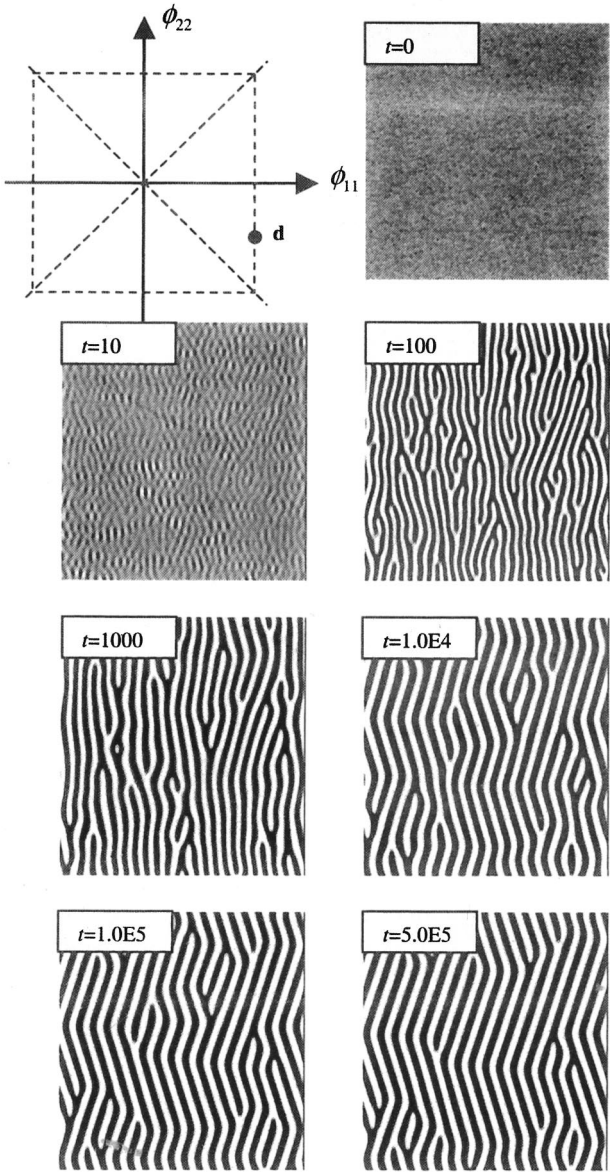

FIG. 6. An evolution sequence for $r=-0.5$.

principal direction that the slope of the surface stress is larger. The larger surface stress slope allows more elastic energy relaxation. Comparing (b) and (c) with (a), we observe that the width of the stripes is roughly the same.

Quite beyond our initial expectation, in (d) $r=-0.5$, we obtain herringbone structures. In (e), $r=-1$ and we obtain tweed structures. The stripes align along the diagonal direction. It is found the stripes turn more close to the diagonal direction when r becomes more negative. We will examine this mesophase transition between the parallel stripes and the herringbones in the next section.

Figure 6 shows the time sequence for $r=-0.5$. The initial condition is random, with average concentration 0.5 plus a fluctuation within 0.001 from the average. $\Omega=2.2$ and $Q=1$, the same as those in Fig. 3. We can still broadly identify three states of evolution: phase separation, size selection, and special ordering. However, the ordering process is much faster. A herringbone structure is obtained within 1.0×10^5.

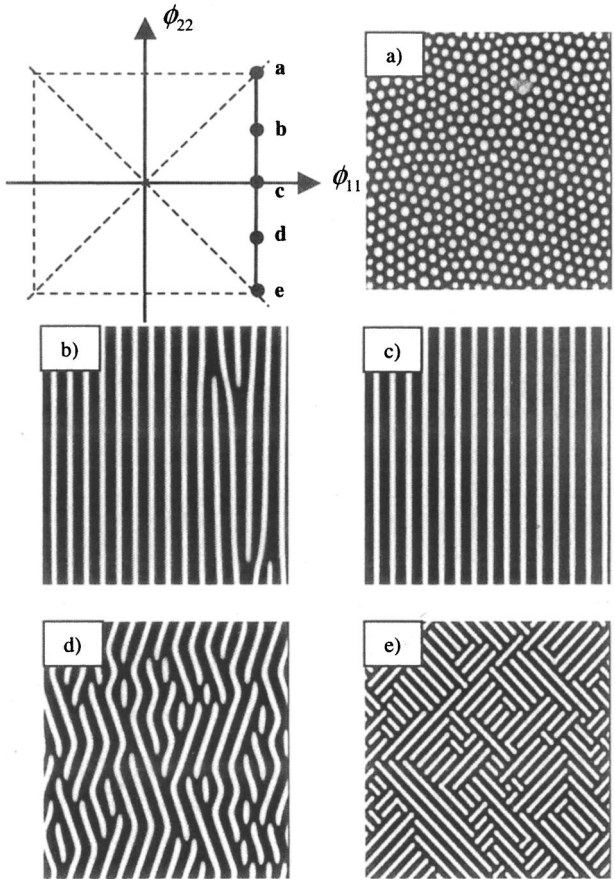

FIG. 7. Various patterns at $t=2.0\times10^5$ under different surface stress anisotropy. The average concentration is 0.4.

Two variants of stripes, with different orientations, can be identified from the patterns. For the given symmetry, the two variants are energy equivalent. The width of the stripes, which is determined by the intrinsic length scale, stabilizes very fast. However, the length of the stripes continues to grow at $t=5\times10^5$.

Figure 7 shows the patterns for average concentration equal to 0.4. The figures are patterns at $t=2.0\times10^5$, initiated at a random concentration. When the surface stress is isotropic, the system forms dots. The dots locally form a triangular lattice, but over long distance form multidomains. Our model predicts that average concentration affects the pattern formation, as observed in experiments.[4] The multidomain and local ordering structures of dots have been found in many other systems, such as block copolymers and Langmuir monolayers. Long-range ordering is difficult to attain. A similar phenomenon also appears in the recently discovered lithographically induced self-assembly (LISA).[29]

Figures 7(b)–7(e) show that surface stress anisotropy can considerably affect the pattern formation: it can change the patterns from dots to stripes. Note the dislocations in Fig. 7(b).

IV. MESOPHASE TRANSITION INDUCED BY SURFACE STRESS ANISOTROPY

Our numerical simulation has revealed a surprising finding. There seems to exist a critical point r_c somewhere be-

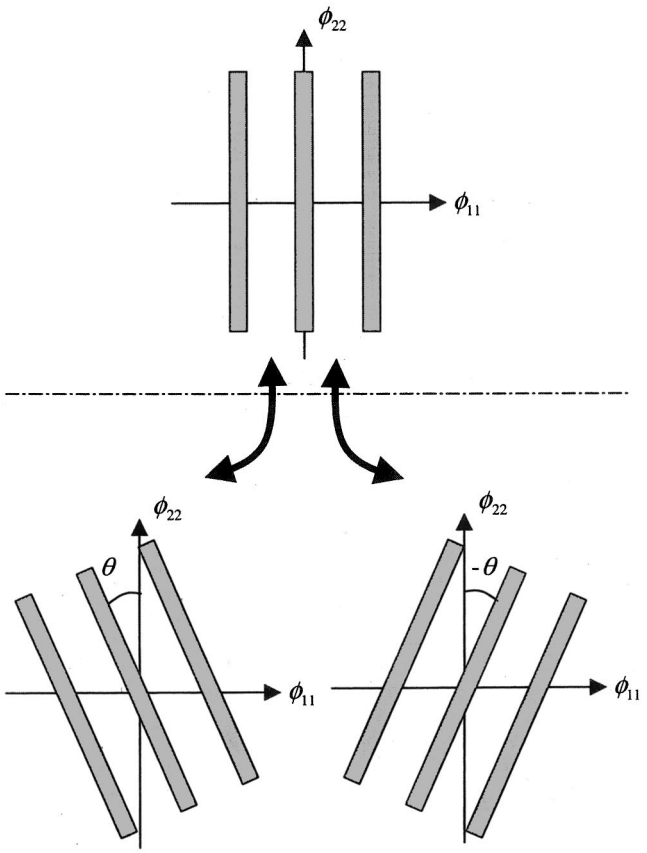

FIG. 8. A mesophase transition induced by surface stress anisotropy.

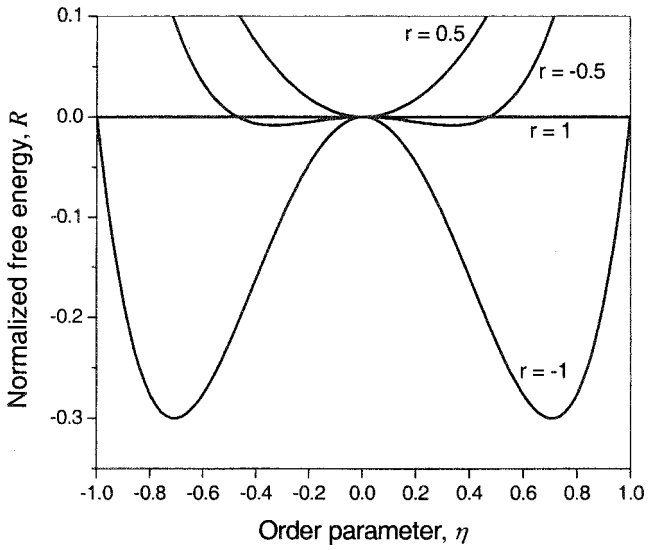

FIG. 9. The normalized free energy R as a function of the order parameter η.

tween $r=-0.5$ and $r=0$. When $r_c<r<1$, the stripes are parallel to the ϕ_{22} direction. When $-1\leqslant r<r_c$, the stripes deviate from the ϕ_{22} direction. The angle between the orientation of the stripes and the ϕ_{22} direction is determined by the value of r. As shown in Fig. 8, the orientations of θ and $-\theta$ are equivalent variants that break the symmetry of the system. In the following we look at the mesophase transition more carefully and show that it follows the Landau theory.[30]

The question is the following: assuming that an arbitrary concentration stripe is formed on the substrate and $r=\phi_{22}/\phi_{11}$ is known, what will be the orientation θ of such a stripe? The stripes should select their orientations to relax the energy of the system as much as possible. The surface stress is a second-rank tensor, so is the slope $\phi_{\alpha\beta}$. According to tensor algebra, the maximum direction for the slope coincides with one of the principal directions of the tensor, namely, the ϕ_{11} direction assuming $|\phi_{11}|\geqslant|\phi_{22}|$ Then why do stripes sometimes deviate from the direction normal to ϕ_{11}? We will give a qualitative answer first, followed by a detailed calculation. When a set of parallel stripes lines up in a direction off the two principal directions of the ϕ tensor, a shear component of the ϕ tensor arises. In the new coordinates that are normal and parallel to the stripes (x_1',x_2'), we denote the tensor components by $\phi'_{\alpha\beta}$. In the cross section (x_1',x_3) of the substrate, the component ϕ_{11} generates a plane strain field and ϕ'_{12} generates an antiplane shear strain field. Both fields contribute to the elastic energy relaxation. The former favors the stripes in the principal direction of the ϕ tensor, and the latter favors the stripes off the principal direction.

The energy per unit area of the system, g_{ave}, is expressed by[17]

$$g_{\text{ave}}=\frac{1}{A}\int_A\left(g(C)+hC_{,\alpha}C_{,\alpha}-\frac{1}{2}\sigma_{3\alpha}u_\alpha\right)dA, \qquad (15)$$

where A is the area of the surface and u_α the displacement in the epilayer. The first two terms in the brackets are isotropic. Let $\eta=\sin\theta$ be the order parameter. A calculation shows that for any concentration modulation, the free energy takes the form

$$g_{\text{ave}}=g_0+R(\eta)g_1, \qquad (16)$$

where g_0 and g_1 $(g_1>0)$ are independent of the orientation η, and R is expressed by

$$R(\eta)=(1-r)[r+(1-2\nu)]\eta^2+\nu(1-r)^2\eta^4. \qquad (17)$$

The preferred orientation is obtained by minimizing g_{ave} or R. We only need to consider $|r|\leqslant 1$ and $|\eta\leqslant 1$. In the expression (17), the coefficient for η^4 is always positive. The coefficient for η^2 is positive when $r>r_c$ and negative when $r<r_c$, where $r_c=-(1-2\nu)$. The function $R(\eta)$ is drawn in Fig. 9. We distinguish the following cases.

(i) When $r=1$, the surface stress is isotropic and $R=0$ for all orientations η. All orientations are energy equivalent, as expected.

(ii) When $r_c<r<1$, the coefficient for η^2 is positive, so that R minimizes at $\eta_{\text{eq}}=0$, corresponding to stripes parallel to ϕ_{22}.

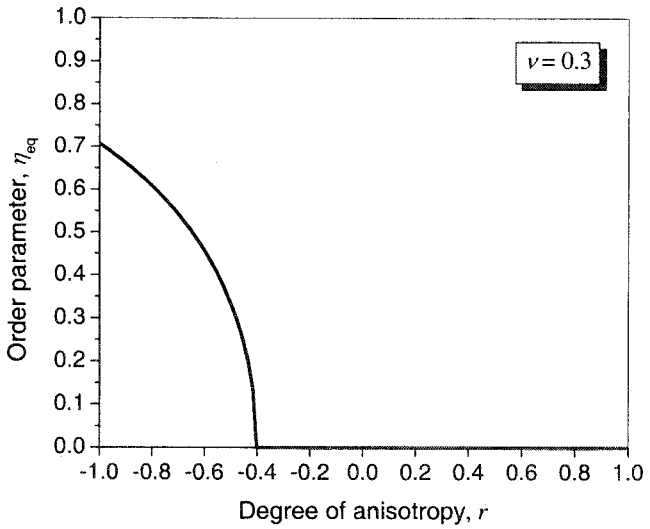

FIG. 10. The equilibrium value of the orientation order parameter η_{eq} as a function of the degree of surface stress anisotropy r.

(iii) When $-1 \leqslant r < r_c$, the coefficient for η^2 is negative, so that R has a local maximum at $\eta=0$ and two minima at

$$\eta_{eq} = \pm \sqrt{\frac{r_c - r}{2\nu(1-r)}}. \tag{18}$$

They correspond to the two orientations obtained in the numerical simulations, Figs. 5–7. In the simulations, we have taken $\nu=0.3$, so that $r_c = -0.4$. The stripes line up in the ϕ_{22} direction for cases **b** and **c**, but form two variants for cases **d** and **e**. Figure 10 plots the relation between the equilibrium orientation η_{eq} and the anisotropy parameter r. The equilibrium orientations agree with those obtained by the dynamic simulations.

V. CONCLUDING REMARKS

A binary epilayer on a solid surface may self-assemble into ordered structures. We have proposed a thermodynamic model to study this phenomenon. The formation of stable concentration patterns requires three ingredients: phase separation, phase coarsening, and phase refining. These ingredients result in a nonlinear diffusion equation, with which we have simulated the entire process of pattern evolution. The surface stress refines and stabilizes the patterns. Without the surface stress, the phases will coarsen as much as possible. However, with the surface stress, the phases reach their equilibrium sizes and become stable. When the surface stress is isotropic, the epilayer forms interwoven stripes or disordered dots, depending on the average concentration. The anisotropy of the surface stress generates two kinds of patterns: parallel stripes and herringbone structures. As the degree of the surface stress anisotropy changes, the epilayer changes from one pattern to the other. Each pattern is a mesophase. A herringbone structure is a mixture of two sets of parallel stripes, which form by breaking the symmetry of the single set of parallel stripes. Taking the stripe orientations as the order parameter, we show that the mesophase transition is of second order and occurs when the degree of surface stress anisotropy reaches a critical value. We hope that experiments will soon succeed in verifying this prediction.

ACKNOWLEDGMENT

This work was supported by the Department of Energy through Contract No. DE-FG02-99ER45787.

*Corresponding author. Present address: Mechanical Engineering, Univ. of Michigan, College of Engineering, 2250 G. G. Brown, 2350 Hayward St., Ann Arbor, MI 48109-2125.

[1] K. Pohl, M. C. Bartelt, J. de la Figuera, N. C. Bartelt, J. Hrbek, and R. Q. Hwang, Nature (London) **397**, 238 (1999).
[2] K. Umezawa, S. Nakanishi, M. Yoshimura, K. Ojima, K. Ueda, and W. M. Gibson, Phys. Rev. B **63**, 35 402 (2001).
[3] E. Wahlström, I. Ekvall, H. Olin, S. Lindgren, and L. Walldén, Phys. Rev. B **60**, 10 699 (1999).
[4] R. Plass, J. A. Last, N. C. Bartelt, and G. L. Kellogg, Nature (London) **412**, 875 (2001).
[5] K. Kern, H. Niebus, A. Schatz, P. Zeppenfeld, J. George, and G. Comsa, Phys. Rev. Lett. **67**, 855 (1991).
[6] R. C. Cammarata, Prog. Surf. Sci. **46**, 1 (1994).
[7] R. C. Cammarata and K. Sieradzki, Annu. Rev. Mater. Sci. **24**, 215 (1994).
[8] H. Ibach, Surf. Sci. Rep. **29**, 193 (1997).
[9] P. J. Feibelman, Phys. Rev. B **51**, 17 867 (1995).
[10] R. J. Needs and M. J. Mansfield, J. Phys.: Condens. Matter **1**, 7555 (1989).
[11] H. J. Gossmann, J. C. Beam, L. C. Feldman, E. G. McRac, and I. K. Robinson, Phys. Rev. Lett. **55**, 1106 (1985).
[12] D. Wolf, Phys. Rev. Lett. **70**, 627 (1993).
[13] O. L. Alerhand, D. Vanderbilt, R. D. Meade, and J. D. Joannopoulos, Phys. Rev. Lett. **61**, 1973 (1988).
[14] F. K. Men, W. E. Packard, and M. B. Webb, Phys. Rev. Lett. **61**, 2469 (1988).
[15] S. Narasimhan and D. Vanderbilt, Phys. Rev. Lett. **69**, 1564 (1992).
[16] J. V. Barth, H. Brune, G. Ertl, and R. G. Behm, Phys. Rev. B **42**, 9307 (1990).
[17] Z. Suo and W. Lu, J. Mech. Phys. Solids **48**, 211 (2000).
[18] W. Lu and Z. Suo, Z. Metallkd. **90**, 956 (1999).
[19] J. W. Cahn and J. E. Hilliard, J. Chem. Phys. **28**, 258 (1958).
[20] L. Q. Chen and Y. Wang, J. Optim. Theory Appl. **48**, 13 (1996).
[21] L. Q. Chen and A. G. Khachaturyan, Phys. Rev. Lett. **70**, 1477 (1993).
[22] Z. Suo and W. Lu, in *Multi-Scale Deformation and Fracture in Materials and Structures—The James R. Rice 60th Anniversary Volume*, edited by T.-J. Chuang and J. W. Rudnicki (Kluwer Academic, Dordrecht, 2000), pp. 107–122.

[23] W. Lu and Z. Suo, J. Mech. Phys. Solids **49**, 1937 (2001).
[24] Z. Suo and W. Lu, J. Nanopart. Res. **2**, 333 (2000).
[25] J. W. Cahn, Acta Metall. **28**, 1333 (1980).
[26] J. W. Cahn, Acta Metall. **9**, 795 (1961).
[27] K. L. Johnson, *Contact Mechanics* (Cambridge University Press, Cambridge, England, 1985).
[28] M. Seul and D. Andelman, Science **267**, 476 (1995).
[29] S. Y. Chou and L. Zhuang, J. Vac. Sci. Technol. B **17**, 3197 (1999).
[30] L. D. Landau and E. M. Lifshitz, *Statistical Physic*, 3rd ed. (Butterworth Heinemann, London, 1980), Chap. XIV.